Loss of AP-3 function affects spontaneous and evoked release at hippocampal mossy fiber synapses

Anita Scheuber*, Rachel Rudge†‡, Lydia Danglot†‡, Graca Raposo§, Thomas Binz¶, Jean-Christophe Poncer*, and Thierry Galli†‖

*Institut National de la Santé et de la Recherche Médicale, Université Pierre et Marie Curie–Paris 6, Unité Mixte de Recherche 739, Cortex and Epilepsy, F-75013 Paris, France; †Membrane Traffic in Neuronal and Epithelial Morphogenesis, Institut National de la Santé et de la Recherche Médicale Avenir Team, F-75005 Paris, France; ‡Institut Jacques Monod, Centre National de la Recherche Scientifique, Unité Mixte de Recherche 7592, Université Paris 6, Université Paris 7, F-75005 Paris, France; §Structure and Membrane Compartments, Centre National de la Recherche Scientifique, Unité Mixte de Recherche 144, Institut Curie, F-75005 Paris, France; and ¶Institute of Biochemistry, Medical School Hannover, D-30625 Hannover, Germany

Edited by Pietro V. De Camilli, Yale University School of Medicine, New Haven, CT, and approved September 1, 2006 (received for review April 28, 2006)

Synaptic vesicle (SV) exocytosis mediating neurotransmitter release occurs spontaneously at low intraterminal calcium concentrations and is stimulated by a rise in intracellular calcium. Exocytosis is compensated for by the reformation of vesicles at plasma membrane and endosomes. Although the adaptor complex AP-3 was proposed to be involved in the formation of SVs from endosomes, whether its function has an indirect effect on exocytosis remains unknown. Using *mocha* mice, which are deficient in functional AP-3, we identify an AP-3-dependent tetanus neurotoxin-resistant asynchronous release that can be evoked at hippocampal mossy fiber (MF) synapses. Presynaptic targeting of the tetanus neurotoxin-resistant vesicle soluble *N*-ethylmaleimide-sensitive factor attachment protein receptor (SNARE) tetanus neurotoxin-insensitive vesicle-associated membrane protein (TI-VAMP) is lost in *mocha* hippocampal MF terminals, whereas the localization of synaptobrevin 2 is unaffected. In addition, quantal release in *mocha* cultures is more frequent and more sensitive to sucrose. We conclude that lack of AP-3 results in more constitutive secretion and loss of an asynchronous evoked release component, suggesting an important function of AP-3 in regulating SV exocytosis at MF terminals.

hippocampus | neurotransmitter release | tetanus neurotoxin

The release of a neurotransmitter at the synapse requires the fusion and recycling of synaptic vesicles (SVs). The fusion of SVs with the plasma membrane depends on the formation of soluble *N*-ethylmaleimide-sensitive factor attachment protein receptor (SNARE) complexes between vesicle SNAREs and plasma membrane SNAREs, as demonstrated by the striking sensitivity of neurotransmitter release to clostridial neurotoxins, particularly tetanus neurotoxin (TeNT; for a review, see ref. 1). Several models of the recycling of SVs have been proposed: endosomal recycling, SV budding from the plasma membrane (2), and kiss-and-run and kiss-and-stay (for a review, see ref. 3). Endosomal recycling involves the molecular coat AP-3, as suggested from experiments in neuroendocrine cells (4), but the importance of AP-3 in neurotransmitter release is still unclear. AP-3 is composed of four subunits, and two different AP-3 complexes are expressed in brain, the ubiquitous AP-3A, composed of the δ, σ3, β3A, and μ3A subunits; and the neuronal-specific AP-3B, composed of the δ, σ3, β3B, and μ3B subunits (5, 6). *mocha* mice are deficient for the δ subunit and therefore lack both AP-3A and AP-3B complexes. These mice have neurological disorders, including hyperactivity and spontaneous seizures. In this paper, we set out to understand the importance of AP-3 function in neurotransmitter release by characterizing basal and evoked neurotransmitter release in *mocha* mice.

Results

Asynchronous Release Evoked at Mossy Fiber (MF) Terminals Is Lost in *mocha* Mice. AP-3 is particularly concentrated in the hilus and CA3 region of the hippocampus in heterozygous control (+/−) mice (Fig. 5*a*, which is published as supporting information on the PNAS web site)]. Therefore, to assess the role of AP-3 in neurotransmitter release, we compared synaptic transmission at MF-CA3 synapses in organotypic hippocampal cultures from *mocha* (−/−) and heterozygous control (+/−) littermates (Fig. 1*a*). We first examined Ca^{2+}-dependent release evoked by MF stimulation. A stimulating electrode placed at the hilar border of the granule cell layer reliably evoked large postsynaptic currents (PSCs) that were specifically suppressed by the group 2 metabotropic glutamate receptor agonist DCG-IV (Fig. 1*b*; ref. 7). The amplitude of the PSCs gradually increased with stimulation intensities ranging from 15 to 600 V·μs. The correlation between the average charge of the PSCs and the stimulation intensity was not significantly different in cultures prepared from control vs. *mocha* mice (Fig. 1*c*). Cleavage of the SV SNARE synaptobrevin 2 (Syb2) by preincubation of the cultures with TeNT for >72 h caused a dramatic reduction in transmitter release evoked by MF stimulation. In cultures prepared from control mice, stimuli up to 2,000 V·μs evoked small unreliable PSCs, reminiscent of evoked transmission in cultured hippocampal neurons from Syb2 knockout mice (8). Release at stimulated synapses was usually asynchronous and occurred within ≈200 ms after stimulation with an average probability of 0.26 ± 0.05 at the highest stimulation intensities ($n = 7$). In contrast, no PSC could be evoked by MF stimulation in cultures prepared from *mocha* littermate mice.

Loss of Presynaptic TI-VAMP in MF Terminals. Our observations may reflect the contribution of a TeNT-insensitive AP-3-dependent pathway of transmitter release at MF terminals. We have shown that tetanus neurotoxin-insensitive vesicle-associated membrane protein (TI-VAMP) (*i*) is present at a high level in SVs at MF terminals (9), (*ii*) interacts with the δ subunit of the AP-3 complex, and (*iii*) is mistargeted in *mocha* fibroblasts (10). TI-VAMP is therefore the best candidate v-SNARE to support TeNT-resistant vesicle exocytosis at MF terminals. Because TI-VAMP is not expressed at Schaffer collateral terminals onto rat CA1 pyramidal cells (ref. 9; Fig. 5*a*), we anticipated this form of exocytosis may not be observed at these synapses. Consistent with this prediction, evoked release was entirely impaired by TeNT at Schaffer collateral synapses onto CA1 pyramidal cells in control mice (Fig. 1 *a* and *b*).

Author contributions: A.S., R.R., and L.D. contributed equally to this work; J.-C.P. and T.G. designed research; A.S., R.R., L.D., G.R., and J.-C.P. performed research; T.B. contributed new reagents/analytic tools; A.S., R.R., L.D., J.-C.P., and T.G. analyzed data; and A.S., R.R., L.D., G.R., J.-C.P., and T.G. wrote the paper.

The authors declare no conflict of interest.

This article is a PNAS direct submission.

Abbreviations: SV, synaptic vesicle; TeNT, tetanus neurotoxin; MF, mossy fiber; PSC, postsynaptic current; Syb2, synaptobrevin 2; BFA, brefeldin A; mEPSC, miniature excitatory PSC; Syp, synaptophysin; SNARE, soluble *N*-ethylmaleimide-sensitive factor attachment protein receptor; TI-VAMP, tetanus neurotoxin-insensitive vesicle-associated membrane protein.

‖To whom correspondence should be addressed. E-mail: thierry@tgalli.net.

www.pnas.org/cgi/doi/10.1073/pnas.0603511103

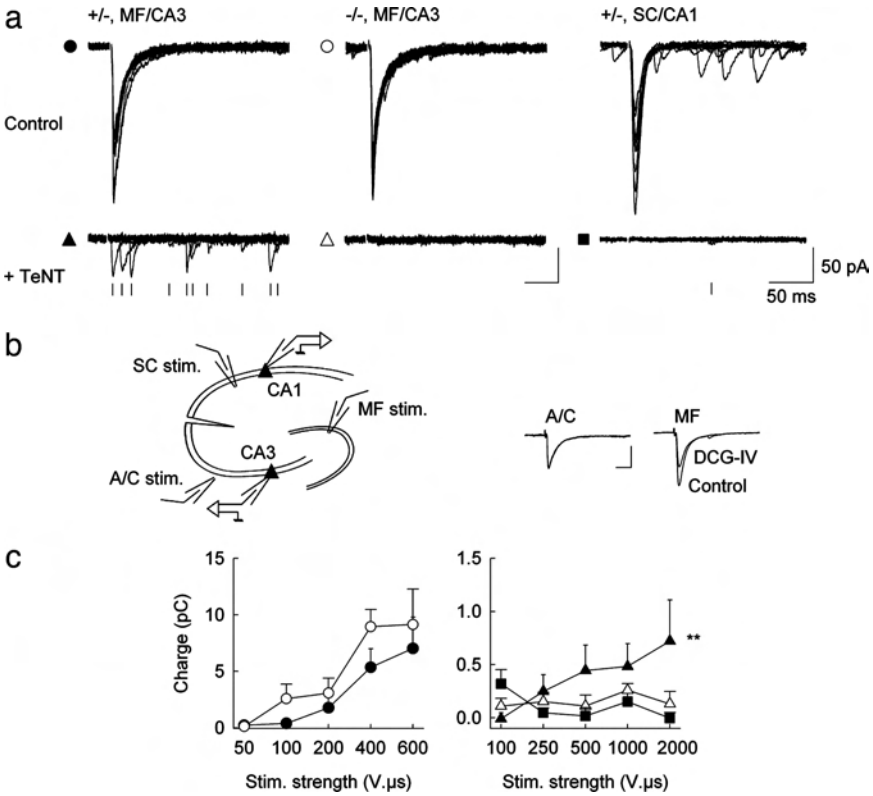

Fig. 1. Evoked synaptic transmission in slice cultures prepared from control and *mocha* mice. (*a*) PSCs evoked in CA3 pyramidal cells by MF stimulation. Ten superimposed sample traces are shown for maximal stimulation intensity. (*Upper*) Control cultures; (*Lower*) cultures treated for at least 72 h with TeNT (500 ng/ml). After TeNT treatment, unreliable asynchronous responses (marked with a tick) can be detected in control (+/−) but not mocha (−/−) cultures. EPSCs evoked by Schaffer collateral stimulation in CA1 cells are also completely abolished by prior incubation with TeNT. (*b*) Stimulation arrangement. MF were stimulated with a patch pipette located at the hilar border of the granule cell layer (MF stim.). Associational/commissural fibers (A/C) were stimulated in stratum oriens. Responses to either stimulation were distinguishable by their sensitivity to DCG-IV (1 μM). (*c*) Comparison of responses (integrated over 200 ms of the stimulus artifact) evoked by increasing MF stimulations in control vs. mocha cultures or by SC stimulation in CA1 cells. (*Left*) in control cultures, no significant difference could be detected between control cells (filled circles) and mocha CA3 cells (open circles, $n = 4$ and 7 cells, respectively; two-way ANOVA; $P > 0.05$). (*Right*) After treatment with TeNT, responses were evoked in control CA3 cells (filled triangles) but not in mocha CA3 cells (open triangles) or control CA1 cells (filled squares, $n = 7$, 11, and 5 cells, respectively; two-way ANOVA; $P < 0.02$ for control CA3 vs. mocha CA3 or control CA1 and $P > 0.05$ for mocha CA3 vs. control CA1).

We therefore compared TI-VAMP localization in hippocampal sections from control and *mocha* mice. In the CA3 and dentate gyrus areas of control mice, TI-VAMP was localized in the MF terminals, as demonstrated by its colocalization with the presynaptic marker synaptophysin (Syp, Figs. 2*a* and 5*a*). This was further confirmed in cultured granule cells, because we found that 67.20 ± 6.65% of TI-VAMP positive punctae were also Syp-positive (Fig. 6*a*, which is published as supporting information on the PNAS web site). However, in *mocha* sections, TI-VAMP labeling in MFs was completely lost (Figs. 2*a* and 5*b*). Thus, AP-3 is required for the presynaptic targeting of TI-VAMP to MF terminals. In contrast, Syb2 localization was unchanged in brain sections from *mocha* mice as compared with control (Fig. 2*b*), suggesting that the presynaptic targeting of Syb2 is independent of AP-3. Other SV proteins, including Rab3a, synaptotagmin 1, showed a presynaptic targeting similar in control and *mocha* mice (Fig. 5*b* and L.D. and T.G., unpublished observations). Neurite outgrowth and TI-VAMP localization to the growth cone were unaffected in differentiating mocha neurons (see *Supporting Text* and Fig. 7, which are published as supporting information on the PNAS web site). Together, these results suggest that a form of TeNT-insensitive AP-3-dependent evoked release exists at MF-CA3 synapses, which likely involves TI-VAMP as a v-SNARE.

TI-VAMP Is Blocked in the Cell Body of *mocha* Neurons. We then examined the subcellular localization of TI-VAMP in *mocha* hippocampal granule cells from which MFs originate. We found that TI-VAMP accumulated in the cell bodies of granule cells, as shown by colocalization with VAMP4, a vesicular SNARE located in early endosomes (11, 12) and the trans-Golgi network (ref. 13; Fig. 2*d*). However, the AP-3-dependent sorting of TI-VAMP in the perinuclear VAMP4-positive compartment may not be specific to granule cells, because a strong colocalization of TI-VAMP and VAMP4 was also found in the *mocha* CA3 pyramidal cells (Fig. 2*c*). The accumulation of TI-VAMP in cell bodies in *mocha* neurons was also observed in cultured hippocampal pyramidal neurons by immunolabeling (Fig. 6*b*), as well as immunogold labeling in ultrathin cryosections analyzed by electron microscopy (Fig. 6*c*). TI-VAMP labeling in *mocha* neurons was found restricted to the cytosolic side of Golgi cisternea, whereas in control pyramidal neurons, TI-VAMP labeled vesicles and the plasma membrane, consistent with its function as a secretory v-SNARE in control but not *mocha* neurons. Therefore, an AP-3-dependent sorting of TI-VAMP at the level of a VAMP4-positive perinuclear compartment is required for the proper targeting of TI-VAMP.

Increased Basal Release in Mocha and Brefeldin A (BFA)-Treated MF Terminals. We then asked whether the lack of AP-3 and TI-VAMP may impact Ca^{2+}-independent constitutive release at MF terminals from *mocha* mice. Miniature excitatory PSCs (mEPSCs) were recorded from CA3 pyramidal cells in slice cultures prepared from control and *mocha* littermates. In cultures from *mocha* mice, the

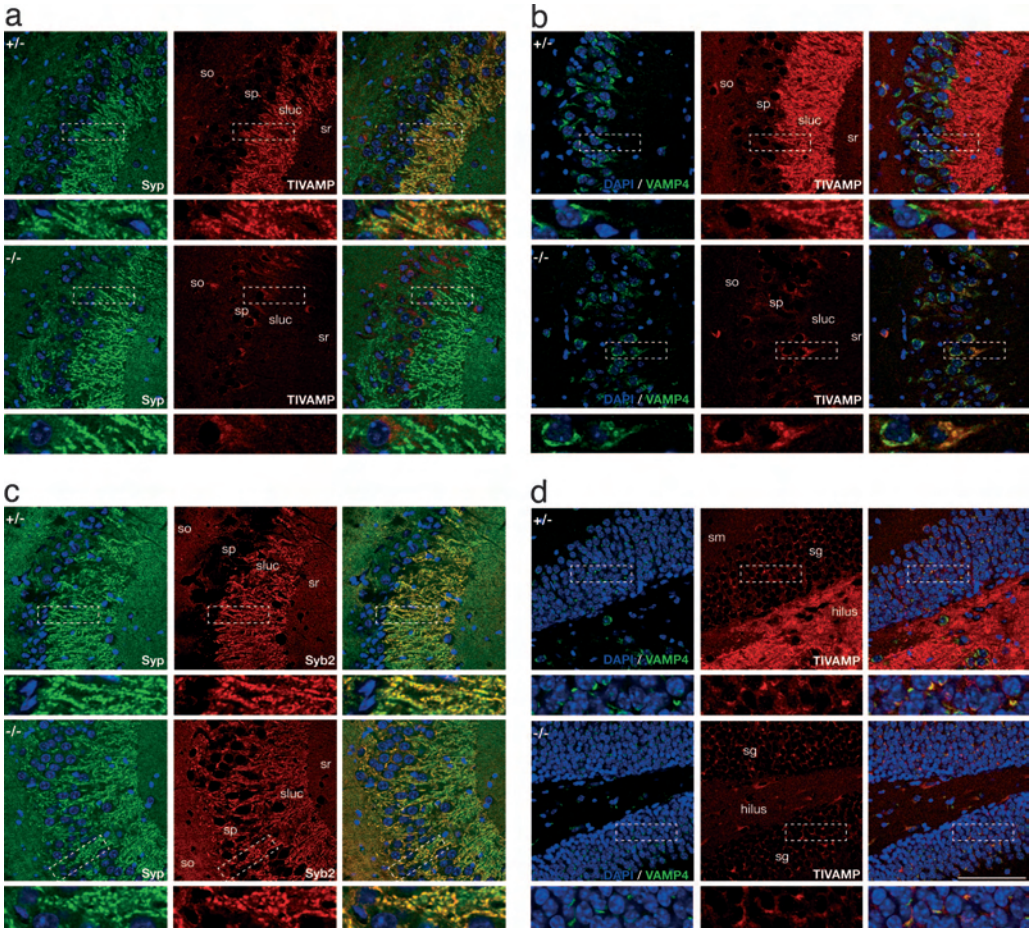

Fig. 2. TI-VAMP is absent from MF terminals and accumulates in the cell body of *mocha* neurons. Fifty-micrometer vibratome sections from adult control (+/−) and *mocha* (−/−) mice were labeled with DAPI (blue) and monoclonal antibodies against TI-VAMP or Syb2, polyclonal antibodies against Syp or VAMP4. (*a*) TI-VAMP is lost from the terminals of granule cells (mossy synapses) innervating CA3 pyramidal cells in *mocha* brain. A dense signal for Syp (green) is detected throughout the CA3 region in stratum oriens (so), stratum pyramidale (sp), and stratum radiatum (sr) in control (+/−) hippocampus. The strong immunofluorescence presented in the stratum lucidum (sluc) corresponds to MF terminals innervating CA3 pyramidal dendrites. Lower images are magnifications of the boxed windows. In control (+/−) mice, confocal images show that TI-VAMP (red) immunoreactivity colocalizes in mossy synapses with Syp puncta in sluc. However, in mocha (−/−) mice, TI-VAMP is not detected in presynaptic terminals (sluc) of granule cells, whereas a faint immunofluorescence is detected in pyramidal cell soma (boxed window in *a* and *c*). (*b*) Syb2 localization is unaffected in the *mocha* hippocampus. As for Syp immunoreactivity, Syb2 is detected in control and *mocha* mice throughout so, sp, sluc, and sr. (*c* and *d*) TI-VAMP is mislocalized in the granule cells of mocha mice. In control mice, TI-VAMP is present in MF in both the lucidum (*c*) and the hilus of the dentate gyrus (*d*). In *mocha* mice, the strong labeling of the lucidum and hilus in the dentate gyrus is not present. Double labeling of TI-VAMP and VAMP4 shows that the remaining TI-VAMP colocalizes with VAMP4 in the cell bodies of pyramidal (sp) and granule cells [stratum granulosum (sg)]. (Scale bar, 100 μm.)

frequency of mEPSCs was ≈2-fold higher than in control cultures (3.22 ± 0.55 vs. 1.66 ± 0.72 Hz, $P < 0.03$; Fig. 3*a*). However, their mean amplitude was unchanged (19.44 ± 1.73 vs. 18.97 ± 3.32 pA, $P = 0.91$), as were their rise time (10–90% of peak, 1.59 ± 0.09 vs. 1.45 ± 0.19 ms, $P = 0.32$) and decay time constant (3.86 ± 0.12 vs. 3.37 ± 0.24 ms, $P = 0.14$; Fig. 3 *b* and *c*). These results suggest the lack of AP-3 did not alter the rate of fusion pore opening or the number of postsynaptic receptors at excitatory synapses onto CA3 pyramidal cells. In addition, the higher mEPSC frequency in *mocha* cultures was not affected by the NMDA receptor antagonist 2-amino-5-phosphonovaleric acid (A.S. and J.-C.P., unpublished observations), suggesting it did not reflect a greater activation of presynaptic NMDA receptors (14, 15) because of the lack of Zn release from MF terminals in *mocha* mice (16, 17). After 72-h incubation with TeNT, mEPSC frequency in control cultures was reduced by ≈84% (to 0.27 ± 0.04 Hz, $n = 9$; Fig. 3*d*), with no apparent change in their mean amplitude (19.18 ± 0.99 vs. 18.97 ± 3.32 pA, $P = 0.89$), again consistent with observations in cultured hippocampal neurons from Syb2 knockout mice (8). In contrast, quantal release in *mocha* cultures was more resistant to TeNT and was reduced in frequency by only ≈44% (to 1.79 ± 0.56 Hz, $n = 8$). These observations suggest the absence of AP-3 not only increases Ca-independent quantal release but also reduces the effect of TeNT. Apart from TI-VAMP and Syb2, no other v-SNARE protein is known to be present at excitatory synapses on CA3 pyramidal cells. Therefore, we analyzed the penetration and cleavage efficiency of TeNT in the slice cultures. We labeled TeNT-treated slice cultures with DAPI and antibodies against TeNT and SNAP-25. We found that TeNT penetrated throughout *mocha* (Fig. 3*e*) as well as control explants (L.D. and T.G., unpublished observations). Furthermore, although the vast majority of Syb2 was cleaved in control and *mocha* explants after a 72-h incubation with TeNT, a small fraction of Syb2 was still detected by Western blotting. Quantification of the blots revealed twice as much TeNT-resistant Syb2 protein in *mocha* cultures as compared with control (Fig. 3*f*). Treatment with TeNT drastically reduced Syb2 labeling, but the remaining signal corresponded largely to Syb2 present at synapses, as revealed by colocalization with Syp (Fig. 3*g*);

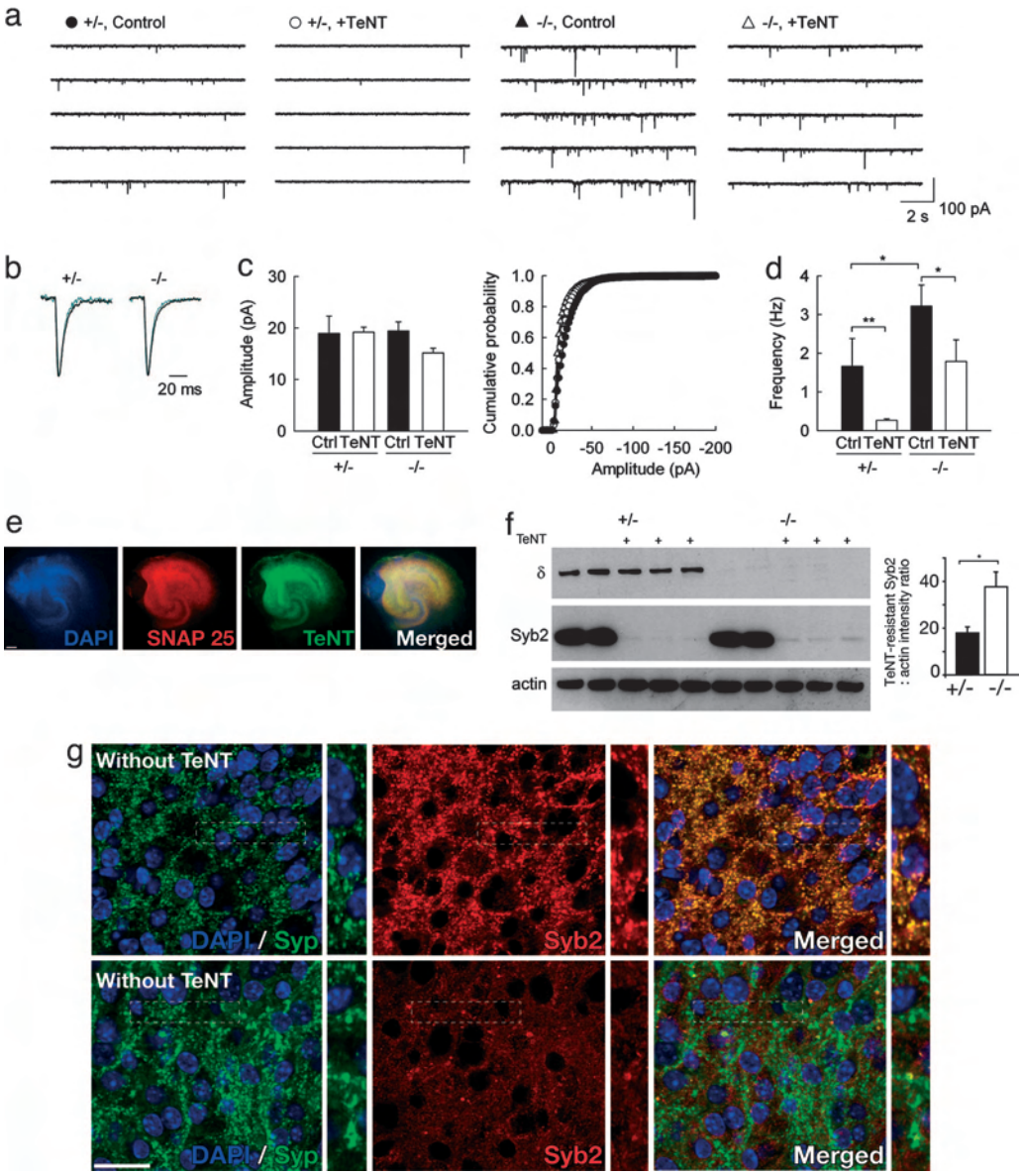

Fig. 3. Ca-independent quantal release at excitatory synapses on CA3 cells in control and *mocha* cultured slices. (*a*) Representative traces of mEPSCs recorded in CA3 pyramidal cells from control (+/−) and *mocha* (−/−) cultures, treated or not with TeNT. (*b*) Averaged mEPSCs (≈100) detected from the above recordings. Black traces, control; blue traces, after TeNT treatment. No difference in either their rate of onset or decay was apparent. (*c*) (*Left*) Average amplitude of mEPSCs recorded in all four conditions. No significant difference was observed ($n = 7$, 9, 11, and 8 cells, respectively; $P > 0.05$). (*Right*) Cumulative amplitude histograms from the same four data sets. The distributions were not significantly different (Kolmogorov–Smirnov test, $P > 0.05$). (*d*) Mean frequencies of mEPSCs were significantly different between control and TeNT-treated cultures in both control and mocha cultures ($P < 0.005$ and $P < 0.05$, respectively). mEPSC frequency was also different in control vs. mocha culture in the absence of TeNT ($P < 0.05$). (*e*) *mocha* culture slices treated with TeNT for 72 h were fixed and labeled with antibodies against SNAP25 (red), TeNT (green), and DAPI (blue). The whole surface of the explant can be visualized by either DAPI (nucleus) or SNAP25 (neuronal plasma membrane). Note that TeNT staining is uniformly distributed, confirming the extended penetration of the toxin. (Scale bar, 200 μm.) (*f*) Culture slices used in electrophysiological recordings were lysed and analyzed by Western blotting with antibodies against AP-3δ, Syb2, and actin (as a loading control). A 72-h treatment with TeNT resulted in efficient cleavage of Syb2, although quantification of the remaining Syb2 revealed a 2-fold increase in TeNT-resistant Syb2 in *mocha* slices [mean ± SEM, control 17.83 ± 2.35, $n = 6$; *mocha* 37.58 ± 6.31, $n = 6$, $P < 0.015$ (Mann–Whitney rank sum test)]. (*g*) *mocha*-cultured slices treated with or without TeNT for 72 h were fixed and labeled with antibodies against Syp (green), Syb2 (red), and DAPI (blue). Note that the remaining Syb2 labeling after TeNT treatment is very faint. The rare remaining Syb2 puncta are mainly synaptic. (Scale bar, 50 μm.)

thus the numerous TeNT-resistant mEPSCs observed in *mocha* are likely to be mediated by a presynaptic pool of Syb2 that resisted the treatment with TeNT.

Newly formed vesicles derived from endosomes disappear with a half life of ≈36 min after treatment with the fungal drug BFA, which specifically targets the AP-3-dependent pathway in PC12 cells (4, 18–20). To test the effect of acute inactivation of the AP-3 pathway, we therefore incubated control hippocampal slices with BFA for ≈2–4 h. In BFA-treated slices, mEPSC frequency was increased by ≈127%, as compared with control (2.59 ± 0.33 vs. 1.14 ± 0.25 Hz, $n = 14$ and 12 cells, respectively; $P < 0.005$; Fig. 8 *a–c*, which is published as supporting information on the PNAS web site). The ratio of synaptic TI-VAMP/synaptic Syp measured by immunolabeling was not significantly altered by BFA neither in the hilus nor in the stratum lucidum (Fig. 8*d*). This is consistent with the fact that longer times may be required to clear TI-VAMP from MF terminals and demonstrate that the *mocha* phenotype can be

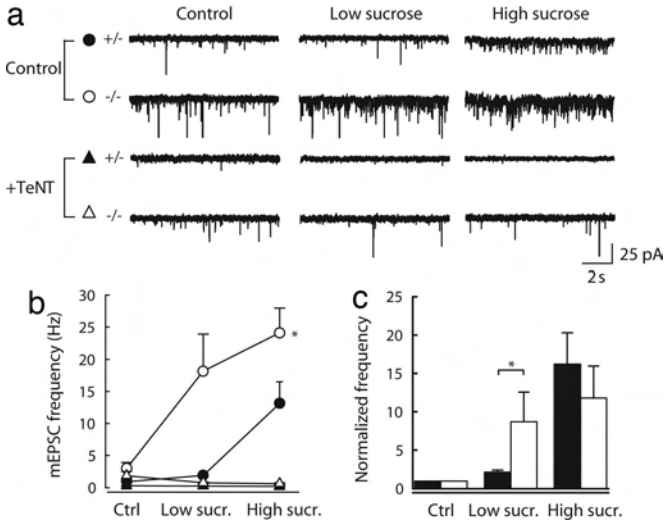

Fig. 4. Differential recruitment of readily releasable vesicles by hypertonic sucrose applications in control vs. *mocha* cultured slices. (*a*) Sample traces from individual recordings of mEPSCs recorded in the presence of tetrodotoxin and an external Ca/Mg ratio of 0.1 before and during application of a 500 mOsm sucrose solution in the presence of a 2.5 ml/min normal artificial cerebrospinal fluid perfusion. High sucrose was applied by pressure injection through a patch pipette to the proximal dendrites of the recorded cell in stratum lucidum. Low sucrose, ≈0.25 psi; high sucrose, 1.5 psi. (*b*) Average frequency of mEPSCs recorded in all conditions. The sensitivity of mEPSC frequency to sucrose was significantly different in control vs. mocha cultures ($n = 4$ and 6 cells, respectively; two-way ANOVA, $P < 0.01$). After treatment with TeNT, sucrose application failed to increase mEPSC frequency ($n = 9$ and 7 cells, respectively). (*c*) Frequencies were normalized to control values, showing a greater relative increase in *mocha* (open bars) compared with control slices (filled bars) upon low-pressure (Mann–Whitney, $P < 0.05$) but not high-pressure application of sucrose ($P = 0.5$).

reproduced by acute pharmacological inactivation of AP-3-dependent SV formation.

Increased Sensitivity of Release to Osmotic Stimulation in *mocha* MF Terminals. Syb2 is resistant to TeNT (21) in SNARE complexes (21) that may be clamped by complexin and synaptotagmin before calcium rise (22). TeNT-resistant Syb2 was associated with release-competent SVs (23, 24). Our previous results could suggest that the lack of AP-3 and TI-VAMP in MF SVs may thus increase the capacity of Syb2 to form TeNT-resistant clamped SNARE complexes, thereby enhancing the probability of calcium-independent fusion at *mocha* MF terminals. To test this hypothesis, we examined the rate of release induced by focal application of a hypertonic solution, because previous studies showed that hypertonic solution specifically recruits readily releasable quanta at hippocampal synapses (25) and stimulates secretion in a calcium independent manner. We thus compared the effects of focal applications of a 0.5 M sucrose solution through a patch pipette positioned in stratum lucidum ≈25 μm away from the somata of the recorded pyramidal cells. Because effective sucrose concentration at release sites may be difficult to control in slice cultures, we used varying injection pressures to compare the sucrose sensitivity of release in *mocha* vs. control cultures. In cells recorded from control cultures, application of sucrose with low pressure (0.25 psi) caused a ≈2-fold increase in mEPSC frequency, whereas at a higher pressure (1.5 psi), a further ≈7-fold increase was observed (Fig. 4). The sensitivity of the release rate to sucrose was significantly increased in recordings from *mocha* cultures; even low-pressure application of sucrose caused a ≈9-fold increase in mEPSC frequency, which was further enhanced by another ≈35% at high pressure (Fig. 4). Interestingly, however, recruitment of readily releasable vesicles by sucrose was disrupted in both control and *mocha* cultures by prior incubation with TeNT, and application of hypertonic solution failed to produce an increase in mEPSC frequency even at high pressure (Fig. 4 *a* and *b*). Taken together, these results suggest that an AP-3-dependent mechanism decreases the sucrose sensitivity of constitutive secretion.

Discussion

mocha mice are deficient for AP-3δ subunit and therefore lack both ubiquitous AP-3A and neuronal AP-3B complexes. Here, we have shown that presynaptic TI-VAMP, a well established AP-3δ cargo (10, 26), is lost in *mocha* CA3 MFs. Other AP-3 cargoes, including the zinc transporter ZnT-3 (16, 17), the chloride channel ClC-3 (27), and the phosphatidylinositol-4-kinase type IIα (28), are mislocalized in *mocha* CA3 MFs. A previous study in ZnT3 knockout mice showed the lack of vesicular zinc in MFs does not significantly affect the MF-associated excitability of CA3 pyramidal cells (29). In addition, we observed that the higher mEPSC frequency in *mocha* cultures was not affected by blocking NMDA receptors, further suggesting that the lack of Zn release from MF terminals in *mocha* mice does not explain the phenotype we observed. Similarly, the lack of MF ClC-3 is unlikely to explain the increased quantal release from *mocha* MF terminals mice. The loss of CIC-3 rather affects acidification of SVs resulting in a slight reduction of quantal size (30). Finally, recent data suggested AP-3 may regulate the volume of large dense-core vesicles in chromaffin cells (31). This, however, is unlikely to apply to MF terminals, because (*i*) we did not observe any change in quantal size in *mocha* cultures, and (*ii*) the pathway of SV reformation largely differs from that of secretory granules, the latter maturing by removal of material from immature secretory granules. Treatment of hippocampal slice cultures with TeNT revealed an asynchronous component of secretion evoked in CA3 pyramidal cells by single stimulation of MFs. This asynchronous release is unlikely to be mediated by the low amount of TeNT-resistant Syb2, because it was not observed in *mocha* cultures, which showed more TeNT-resistant Syb2. Furthermore, this asynchronous component was observed at MF-CA3 but not CA1–CA3 synapses, where TI-VAMP is not expressed. Because no other TeNT-resistant v-SNARE was ever detected at MF terminals, we suggest TI-VAMP likely mediates the asynchronous evoked release unraveled in our experiments. In conclusion, although we cannot exclude that other AP-3 cargoes lost in *mocha* MF terminals may participate to the *mocha* phenotype, the loss of TI-VAMP seems most likely to explain the perturbation of evoked SV release described in the present study.

Asynchronous release was not observed in TeNT-untreated explants, suggesting inactivation of Syb2 may be required for the expression of this asynchronous evoked release. This observation strongly suggests TI-VAMP and Syb2 may both be present on the same rather than distinct SVs. Consistent with this scenario, Syb2 was shown to have a higher rate of SNARE complex assembly than TI-VAMP both *in vitro* and *in vivo* (10), predicting that evoked release mediated by TI-VAMP would be detected only after cleavage of Syb2. In addition, cleavage of Syb2 by TeNT was shown to modify the coupling of intracellular calcium and release-competent vesicles (32), suggesting that removal of TeNT-sensitive v-SNAREs allows for the expression of a secretory machinery that may be hard to observe otherwise. Interestingly, Sr^{+} preferentially stimulates asynchronous release (33), and different synaptotagmin isoforms show different sensitivities to Ca^{2+} and Sr^{+} (34). For instance, Synaptotagmin 1 and 7 have different sensitivities to calcium (35), the latter interacting with TI-VAMP in fibroblasts (36) and showing biochemical properties suitable for a Ca^{2+} sensor for asynchronous release (35, 37, 38). Therefore, we speculate that MF SVs may be equipped with two distinct fusion machineries for exocytosis, one depending on Syb2 and the other on TI-VAMP as a v-SNARE, which may be recruited in different conditions.

We have shown a higher basal calcium-independent release in *mocha* cultures, with no apparent change in quantal size or current

kinetics. This observation strongly argues for a presynaptic difference between control and *mocha* MF-CA3 synapses. This is not the result of a greater density of MF terminals onto *mocha* CA3 pyramidal cells because of axonal sprouting induced in organotypic cultures (39) or a greater contribution of recurrent CA3-CA3 synapses to miniature EPSCs in mocha cultures. Indeed, we found an equal Syp staining in control and *mocha* brain sections and the increased quantal release was also observed upon pharmacological disruption of AP-3 by BFA in acute hippocampal slices. In addition, quantal release evoked by hyperosmotic solution directly applied onto MF terminals was also increased in *mocha* cultures. Therefore, the most likely explanation is that more vesicles are ready to fuse because of the absence of AP-3 and possibly TI-VAMP in *mocha* vs. control MF terminals. How AP-3-dependent sorting may decrease basal release remains to be explored.

In conclusion, our data suggest that the molecular mechanism of transmitter release at MF terminals reaches a high degree of complexity with at least two exocytic v-SNAREs, Syb2 and TI-VAMP. AP-3 function is important for both constitutive as well as evoked release, raising the possibility that specific forms of synaptic plasticity might occur at terminals expressing AP-3 cargoes like TI-VAMP (9).

Materials and Methods

Animals. Heterozygous *mocha* mice were originally obtained from M. Robinson (Cambridge Institute for Medical Research, Cambridge, U.K.) and then bred in-house. The experiments were carried out in accordance with the European Community Council Directive of November 24, 1986 (86/609/EEC). All efforts were made to minimize the number of animals used and their suffering.

Immunofluorescence. *mocha* and control (heterozygous littermates) 1- to 2-month-old mice were anesthetized with 35% chloral hydrate or pentobarbital and perfused through the heart with 4% paraformaldehyde. The dissected brains were fixed overnight in 4% paraformaldehyde in PBS, cut on a vibratome into 30-μm-thick sections, and processed for immunofluorescence as described (9). Confocal laser-scanning microscopy was performed by using an SP2 confocal microscope (Leica Microsystems, Mannheim, Germany). Images were assembled by using Adobe Photoshop (Adobe Systems, San Jose, CA).

Western Blotting. SDS/PAGE analysis was performed by using 4–12% NuPAGE (Invitrogen, Cergy-Pontoise, France) gradient gels and the manufacturer's buffers and then processed for Western blotting. Blots were quantified by using ImageJ (National Institutes of Health, Bethesda, MD), and statistical significance was estimated by using Mann–Whitney rank sum tests performed under SigmaStat (SPSS, Chicago, IL)

Electrophysiological Recordings. Organotypic hippocampal slices from 6-day-old mice were maintained in culture as described (40, 41). After 2–3 days, cultures were preincubated 24 h in serum-free medium and then grown another 3–4 days in fresh serum-free medium with or without TeNT (500 ng/ml) as indicated. Electrophysiological recordings were carried out as described in *Supporting Text*, which is published as supporting information on the PNAS web site. For MF stimulation, the stimulating electrode was positioned at the hilar border of the granule cell layer. For Schaffer collateral stimulation, a cut was made between areas CA3 and CA1, and the electrode was positioned in stratum radiatum $\approx$50–100 μm apart from the recorded cell.

Values are expressed as mean $\pm$ SEM. Statistical significance was estimated by using Mann–Whitney or Wilcoxon rank sum tests or two-way ANOVA performed under SigmaStat (SPSS). Additional details are available in *Supporting Text*.

We are grateful to Lucien Cabanié (Unité Mixte de Recherche 144, Institut Curie, Paris, France) for the production of Cl158.2, Mathilde Chaineau and Agathe Van der Linden for help with *mocha* mice, and Richard Miles for support and critical reading of the manuscript. This work was supported in part by grants from Institut National de la Santé et de la Recherche Médicale (Avenir Program), the European Commission ("Signaling and Traffic" STREP 503229), the Association Française contre les Myopathies, the Ministère de la Recherche (ACI-BDP), the Fondation pour la Recherche Médicale, the Human Frontier Science Program (RGY0027/2001-B101), and the Fondation pour la Recherche sur le Cerveau (to T.G.) R.R. was supported by a postdoctoral fellowship from the Fondation pour la Recherche Médicale, A.S. was supported by a fellowship from the Swiss National Science Foundation, and L.D. was supported by a postdoctoral fellowship from the Association pour la Recherche sur le Cancer.

1. Galli T, Haucke V (2004) *Sci STKE* 2004, re19.
2. Takei K, Mundigl O, Daniell L, De Camilli P (1996) *J Cell Biol* 133:1237–1250.
3. Sudhof TC (2004) *Annu Rev Neurosci* 27:509–547.
4. Faundez V, Horng JT, Kelly RB (1998) *Cell* 93:423–432.
5. Simpson F, Peden AA, Christopoulou L, Robinson MS (1997) *J Cell Biol* 137:835–845.
6. Dell'Angelica EC, Ohno H, Ooi CE, Rabinovich E, Roche KW, Bonifacino JS (1997) *EMBO J* 16:917–928.
7. Kamiya H, Shinozaki H, Yamamoto C (1996) *J Physiol* (*London*) 493:447–455.
8. Schoch S, Deak F, Konigstorfer A, Mozhayeva M, Sara Y, Sudhof TC, Kavalali ET (2001) *Science* 294:1117–1122.
9. Muzerelle A, Alberts P, Martinez-Arca S, Jeannequin O, Lafaye P, Mazie, J-C, Galli T, Gaspar P (2003) *Neuroscience* 122:59–75.
10. Martinez-Arca S, Rudge R, Vacca M, Raposo G, Camonis J, Proux-Gillardeaux V, Daviet L, Formstecher E, Hamburger A, Filippini F, *et al*. (2003) *Proc Natl Acad Sci USA* 100:9011–9016.
11. Mallard F, Tang BL, Galli T, Tenza D, Saint-Pol A, Yue X, Antony C, Hong W, Goud B, Johannes L (2002) *J Cell Biol* 156:653–654.
12. Rizzoli SO, Bethani I, Zwilling D, Wenzel D, Siddiqui TJ, Brandhorst D, Jahn R (2006) *Traffic* 7:1163–1176.
13. Zeng Q, Tran TT, Tan HX, Hong W (2003) *J Biol Chem* 278:23046–23054.
14. Sjostrom PJ, Turrigiano GG, Nelson SB (2003) *Neuron* 39:641–654.
15. Woodhall G, Evans DI, Cunningham MO, Jones RS (2001) *J Neurophysiol* 86:1644–1651.
16. Kantheti P, Qiao X, Diaz ME, Peden AA, Meyer GE, Carskadon SL, Kapfhamer D, Sufalko D, Robinson MS, Noebels JL, *et al.* (1998) *Neuron* 21:111–122.
17. Vogt K, Mellor J, Tong G, Nicoll R (2000) *Neuron* 26:187–196.
18. Faundez V, Horng JT, Kelly RB (1997) *J Cell Biol* 138:505–515.
19. Blagoveshchenskaya AD, Hewitt EW, Cutler DF (1999) *Mol Biol Cell* 10:3979–3990.
20. Salazar G, Love R, Werner E, Doucette MM, Cheng S, Levey A, Faundez V (2004) *Mol Biol Cell* 15:575–587.
21. Hayashi T, McMahon H, Yamasaki S, Binz T, Hata Y, Südhof TC, Niemann H (1994) *EMBO J* 13:5051–5061.
22. Giraudo CG, Eng WS, Melia TJ, Rothman JE (2006) *Science* 313:676–680.
23. Xu T, Binz T, Niemann H, Neher E (1998) *Nat Neurosci* 1:192–200.
24. Lonart G, Sudhof TC (2000) *J Biol Chem* 275:27703–27707.
25. Rosenmund C, Stevens CF (1996) *Neuron* 16:1197–1207.
26. Salazar G, Craige B, Styers ML, Newell-Litwa KA, Doucette MM, Wainer BH, Falcon-Perez JM, Dell'angelica EC, Peden AA, Werner E, *et al.* (2006) *Mol Biol Cell* 17:4014–4026.
27. Salazar G, Love R, Styers ML, Werner E, Peden A, Rodriguez S, Gearing M, Wainer BH, Faundez V (2004) *J Biol Chem* 279:25430–25439.
28. Salazar G, Craige B, Wainer BH, Guo J, De Camilli P, Faundez V (2005) *Mol Biol Cell* 16:3692–3704.
29. Lopantsev V, Wenzel HJ, Cole TB, Palmiter RD, Schwartzkroin PA (2003) *Neuroscience* 116:237–248.
30. Stobrawa SM, Breiderhoff T, Takamori S, Engel D, Schweizer M, Zdebik AA, Bosl MR, Ruether K, Jahn H, Draguhn A, *et al.* (2001) *Neuron* 29:185–196.
31. Grabner CP, Price SD, Lysakowski A, Cahill AL, Fox AP (2006) *Proc Natl Acad Sci USA* 103:10035–10040.
32. Sakaba T, Stein A, Jahn R, Neher E (2005) *Science* 309:491–494.
33. Goda Y, Stevens CF (1994) *Proc Natl Acad Sci USA* 91:12942–12946.
34. Li C, Ullrich B, Zhang JZ, Anderson RG, Brose N, Sudhof TC (1995) *Nature* 375:594–599.
35. Sugita S, Shin OH, Han WP, Lao Y, Sudhof TC (2002) *EMBO J* 21:270–280.
36. Rao SK, Huynh C, Proux-Gillardeaux V, Galli T, Andrews NW (2004) *J Biol Chem* 279:20471–20479.
37. Sugita S, Han WP, Butz S, Liu XR, FernandezChacon R, Lao Y, Sudhof TC (2001) *Neuron* 30:459–473.
38. Hui E, Bai J, Wang P, Sugimori M, Llinas RR, Chapman ER (2005) *Proc Natl Acad Sci USA* 102:5210–5214.
39. Gutierrez R, Heinemann U (1999) *Brain Res* 815:304–316.
40. Stoppini L, Buchs PA, Muller D (1991) *J Neurosci Methods* 37:173–182.
41. Musleh W, Yaghoubi S, Baudry M (1997) *Brain Res* 770:298–301.

Corrections

CHEMISTRY, BIOPHYSICS. For the article "Assessing implicit models for nonpolar mean solvation forces: The importance of dispersion and volume terms," by Jason A. Wagoner and Nathan A. Baker, which appeared in issue 22, May 30, 2006, of *Proc Natl Acad Sci USA* (103:8331–8336; first published May 18, 2006; 10.1073/pnas.0600118103), the authors note that an error in the implementation of Eq. **10** in the original paper led to improper scaling of the solvent-accessible volume forces for highly exposed surface atoms. The error in the original implementation of Eq. **10** affects Tables 1 and 2 of the original manuscript as well as Tables 3 and 4 and Figs. 2 *B* and *C* and 3 in the original supporting information. Corrected versions of Tables 1 and 2 appear below. A correction to the supporting information has been published online. This error does not affect the conclusions of the article.

Table 1. Optimized 6/12 and WCA implicit solvent nonpolar MF parameter values and goodness-of-fit metrics

	MF model 6/12			MF model WCA		
Parameters	Attractive	Repulsive	Total	Attractive	Repulsive	Total
σ_s, Å	0.89 [0.87–0.91]	1.29 [1.16–1.44]	1.68 [1.57–1.80]	0.8 [0.73–0.86]	1.29 [1.18–1.41]	1.25 [1.16–1.39]
γ, cal·mol^{-1}·Å^{-2}	—	15(1)	1(1)	—	2(1)	0(1)
p, cal·mol^{-1}·Å^{-3}	—	94(2)	55(2)	—	52(2)	55(2)
r	0.88	0.56	0.83	0.84	0.87	0.86
R	0.97	0.91	0.94	0.97	0.94	0.94
χ^2, 10^{-3} kcal^2·mol^{-2}·Å^{-2}	6.99	3.35	6.47	0.56	4.87	4.63

Separate fits of nonpolar solvation MFs were performed as follows: Attractive, a comparison of attractive implicit (Eq. **15**) and attractive explicit; Repulsive, a comparison of repulsive implicit (Eq. **10**) and repulsive explicit; and Total, a comparison of the total implicit (Eq. **21**) and total explicit (Eq. **8**) nonpolar MFs. Where applicable, standard errors are presented in parentheses; 99% confidence intervals (see text) are presented in brackets.

Table 2. Comparison of total solvation energies (kcal/mol) for small alkane solutes

Compound	WCA 1.25	WCA 0.65	OPLS	AMBER	Exp.
Methane	6.40	1.93	2.40	2.69	2.00
Ethane	8.41	2.25	2.63	—	1.83
Propane	10.5	2.84	2.89	3.02	1.96
Butane	11.8	2.93	3.21	3.19	2.08
Pentane	13.7	3.48	3.78	—	2.33
Hexane	15.6	3.90	3.78	—	2.49
Isobutane	12.0	3.16	3.03	3.27	2.52
2-Methylbutane	13.4	3.45	3.51	—	2.38
Neopentane	13.2	3.46	3.23	—	2.50
Cyclopentane	11.3	2.25	2.80	—	1.20
Cyclohexane	13.7	3.18	2.34	—	1.23

WCA energy values were obtained by using the methods described in the text with $\sigma_s = 1.25$ and 0.65 Å. OPLS energies were taken from Gallicchio *et al.* (35) by using values in table 2 of their paper. AMBER energies are from Shirts *et al.* (64), 'van der Waals' values in table II of their paper. Experimental (Exp.) values are from table VII of Cabini *et al.* (65).

www.pnas.org/cgi/doi/10.1073/pnas.0610582103

NEUROSCIENCE. For the article "Loss of AP-3 function affects spontaneous and evoked release at hippocampal mossy fiber synapses," by Anita Scheuber, Rachel Rudge, Lydia Danglot, Graca Raposo, Thomas Binz, Jean-Christophe Poncer, and Thierry Galli, which appeared in issue 44, October 31, 2006, of *Proc Natl Acad Sci USA* (103:16562–16567; first published October 20, 2006; 10.1073/pnas.0603511103), the authors note that Fig. 3*g* was labeled incorrectly. The corrected figure and its legend appear below.

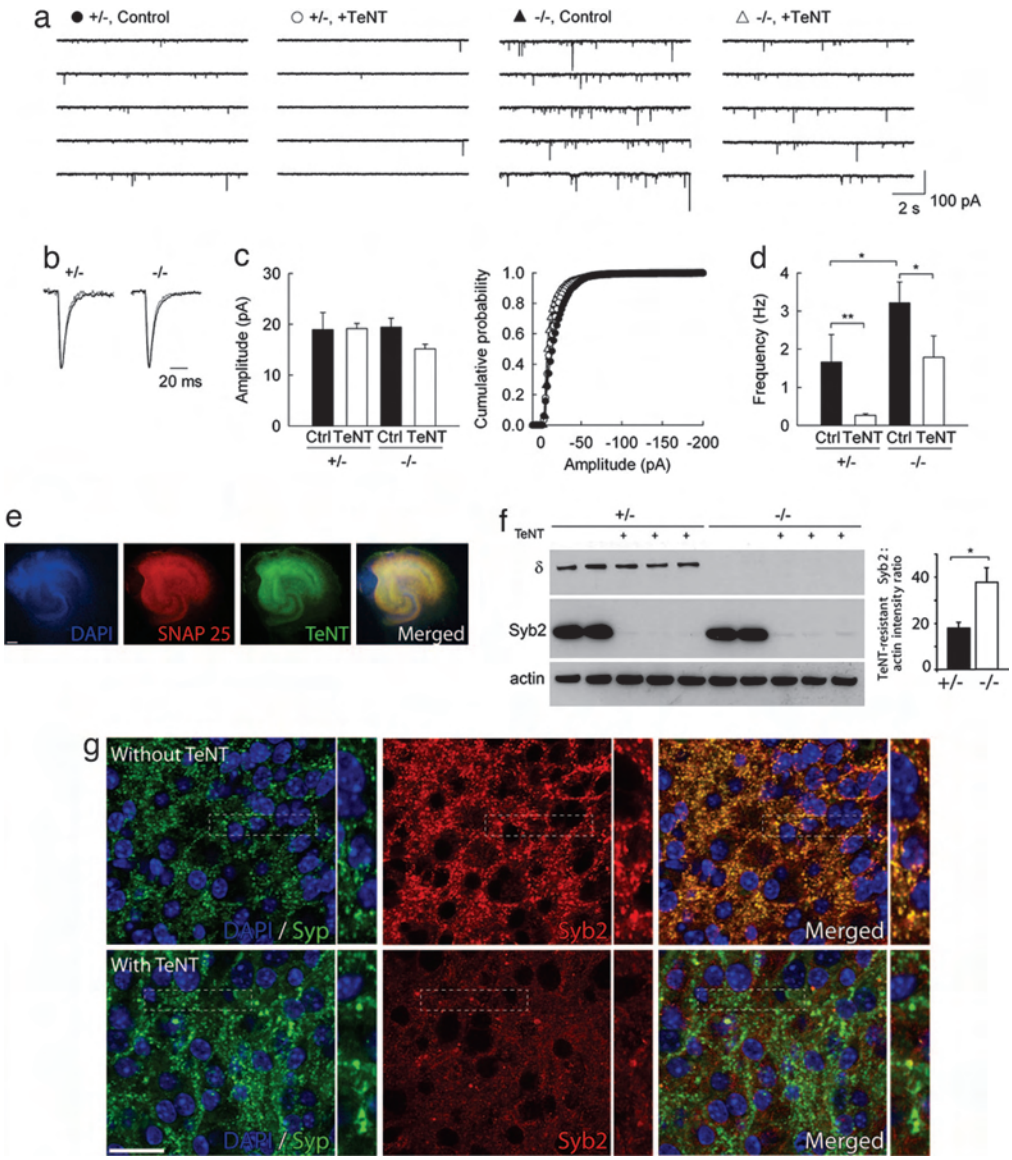

Fig. 3. Ca-independent quantal release at excitatory synapses on CA3 cells in control and *mocha* cultured slices. (*a*) Representative traces of mEPSCs recorded in CA3 pyramidal cells from control (+/−) and *mocha* (−/−) cultures, treated or not with TeNT. (*b*) Averaged mEPSCs (≈100) detected from the above recordings. Black traces, control; blue traces, after TeNT treatment. No difference in their rate of either onset or decay was apparent. (*c*) (*Left*) Average amplitude of mEPSCs recorded in all four conditions. No significant difference was observed ($n = 7$, 9, 11, and 8 cells, respectively; $P > 0.05$). (*Right*) Cumulative amplitude histograms from the same four data sets. The distributions were not significantly different (Kolmogorov–Smirnov test, $P > 0.05$). (*d*) Mean frequencies of mEPSCs were significantly different between control and TeNT-treated cultures in both control and mocha cultures ($P < 0.005$ and $P < 0.05$, respectively). mEPSC frequency was also different in control vs. mocha culture in the absence of TeNT ($P < 0.05$). (*e*) *mocha* culture slices treated with TeNT for 72 h were fixed and labeled with antibodies against SNAP25 (red), TeNT (green), and DAPI (blue). The whole surface of the explant can be visualized by either DAPI (nucleus) or SNAP25 (neuronal plasma membrane). Note that TeNT staining is uniformly distributed, confirming the extended penetration of the toxin. (Scale bar, 200 μm.) (*f*) Culture slices used in electrophysiological recordings were lysed and analyzed by Western blotting with antibodies against AP-3δ, Syb2, and actin (as a loading control). A 72-h treatment with TeNT resulted in efficient cleavage of Syb2, although quantification of the remaining Syb2 revealed a 2-fold increase in TeNT-resistant Syb2 in *mocha* slices [mean ± SEM; control 17.83 ± 2.35, $n = 6$; *mocha* 37.58 ± 6.31, $n = 6$; $P < 0.015$ (Mann–Whitney rank sum test)]. (*g*) *mocha*-cultured slices treated with or without TeNT for 72 h were fixed and labeled with antibodies against Syp (green), Syb2 (red), and DAPI (blue). Note that the remaining Syb2 labeling after TeNT treatment is very faint. The rare remaining Syb2 puncta are mainly synaptic. (Scale bar, 50 μm.)

www.pnas.org/cgi/doi/10.1073/pnas.0611561104

Scheuber *et al*. 10.1073/pnas.0603511103.

Supporting Information

Files in this Data Supplement:

a.

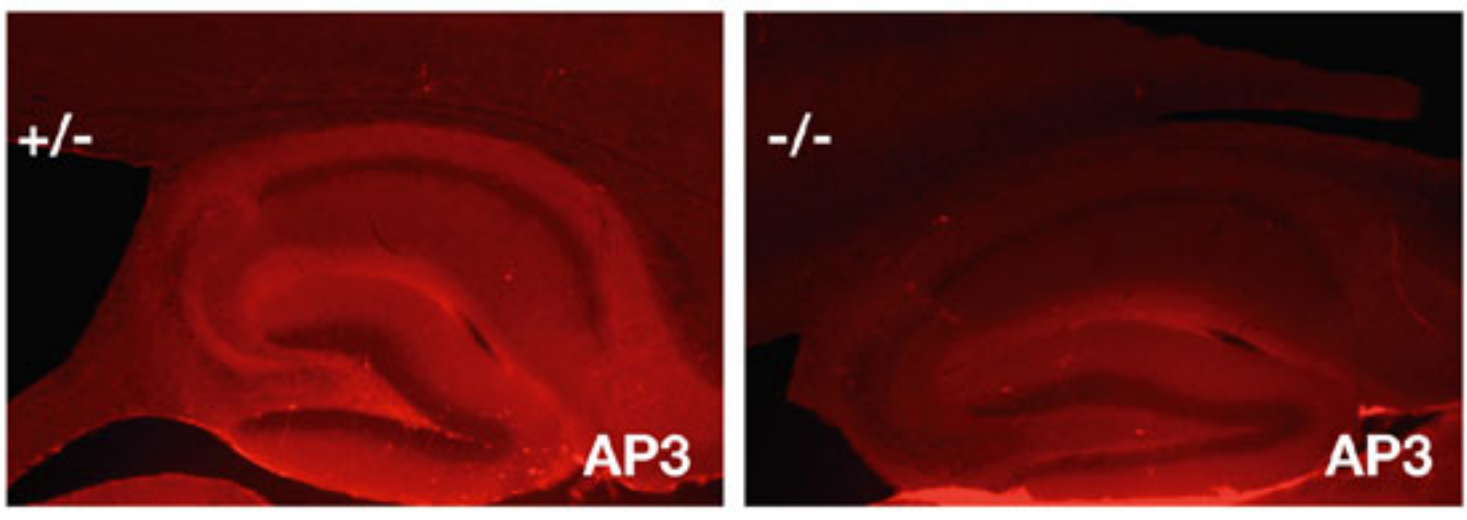
+/-
AP3
-/-
AP3

b.

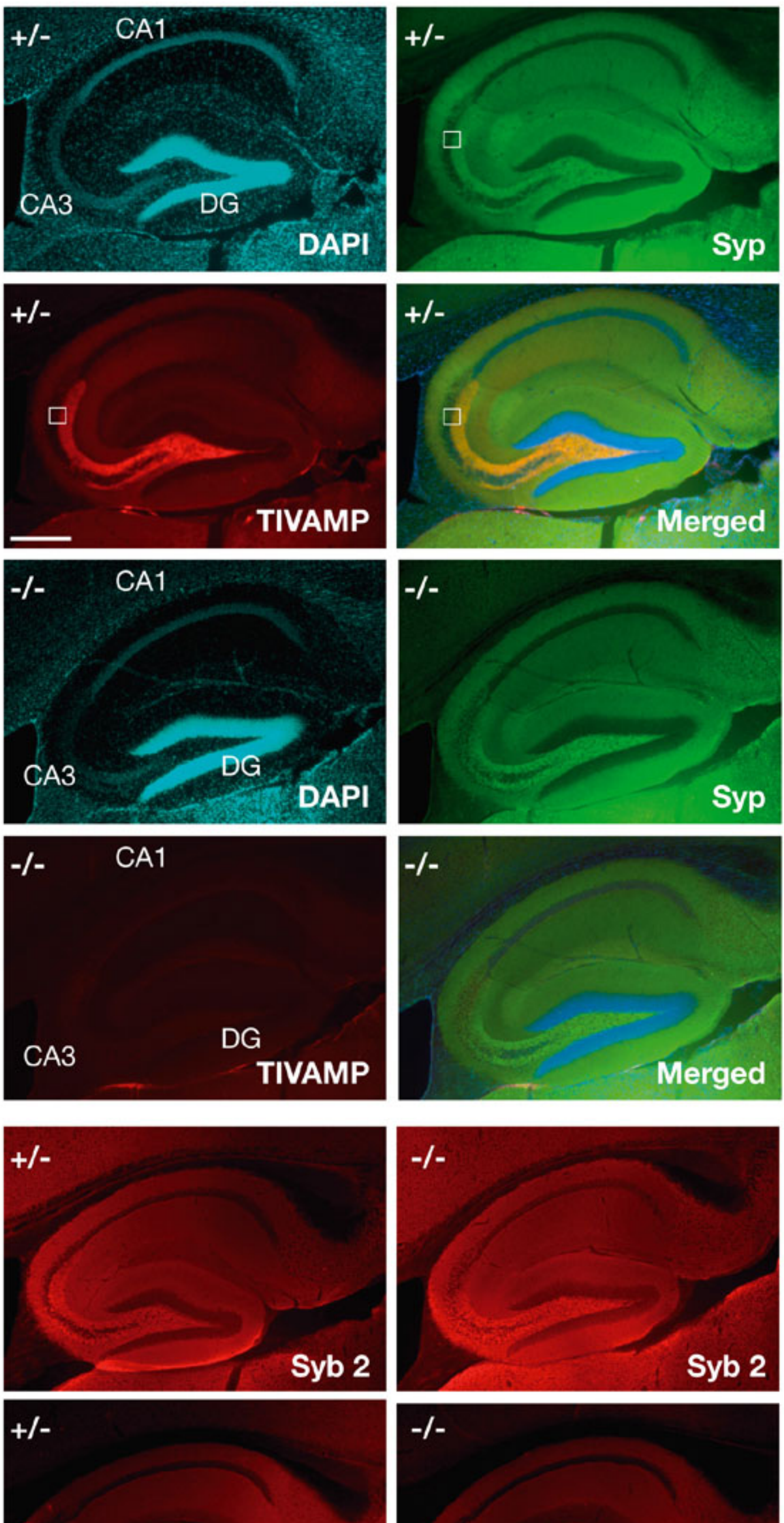
+/-
CA1
CA3
DG
DAPI
+/-
Syp
+/-
TIVAMP
+/-
Merged
-/-
CA1
CA3
DG
DAPI
-/-
Syp
-/-
CA1
CA3
DG
TIVAMP
-/-
Merged

c.

+/-
Syb 2
-/-
Syb 2
+/-
Rab 3a
-/-
Rab 3a

Fig. 5. TI-VAMP and synaptic proteins localization in the whole hippocampus of control and *mocha* mice. (*a*) AP3δ (red) is expressed in the hilus in the dentate gyrus (DG) and in stratum lucidum in the CA3 region of control (+/-)but not in *mocha* (-/-) mice. (*b*) TI-VAMP (red) is mainly expressed by granule cells in presynaptic terminals of the hilus in the DG and in stratum lucidum in CA3 region and faint or absent in pyramidal terminals of the CA1 region in control (+/-) mice. TI-VAMP expression shows a strikingly different pattern in mocha (-/-) mice. Syp immunoreactivity (green) is similar in both mice. The nuclei are labeled with DAPI (blue). (Scale bar = 200 μm.) The boxed region corresponds to the field seen in Fig. 1 at high magnification. (*c*) Distribution patterns of synaptic vesicle proteins were assayed in control and *mocha* mice. No major default was noticed for Syb2 and Rab3a (red) immunoreactivities between the two populations of mice.

a

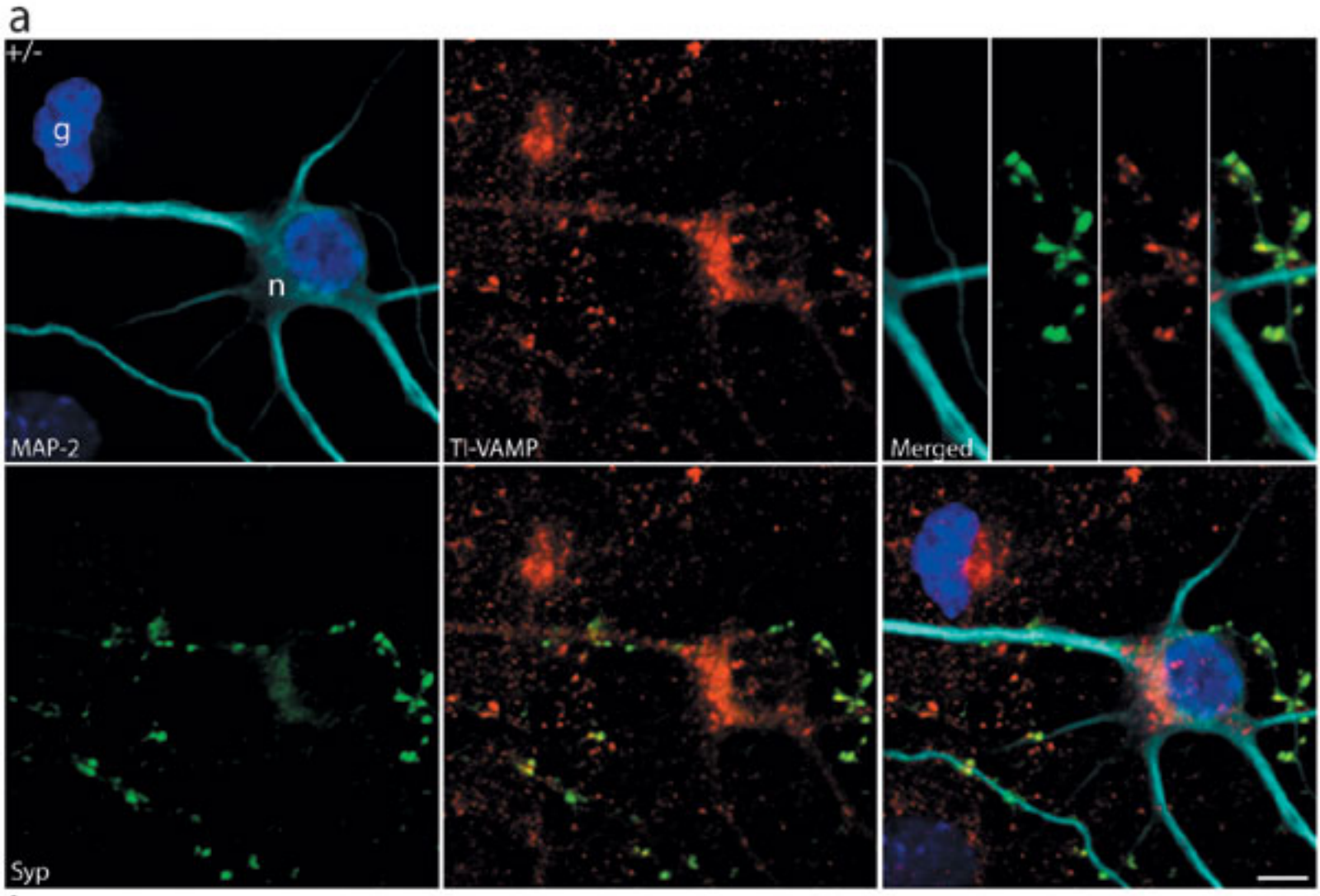
+/-
g
n
MAP-2
Tl-VAMP
Merged
Syp

b

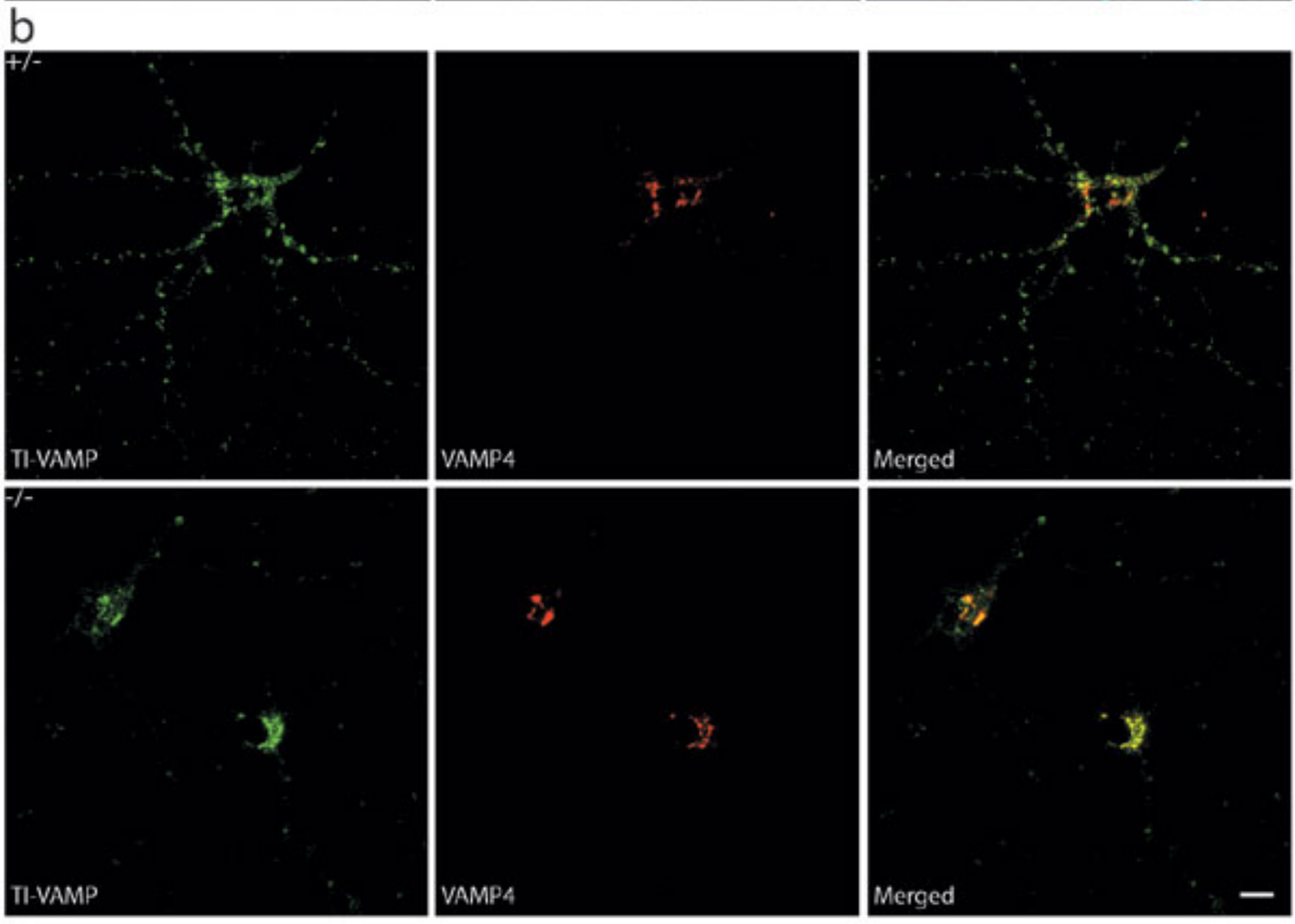
+/-
Tl-VAMP
VAMP4
Merged
-/-
Tl-VAMP
VAMP4
Merged

C

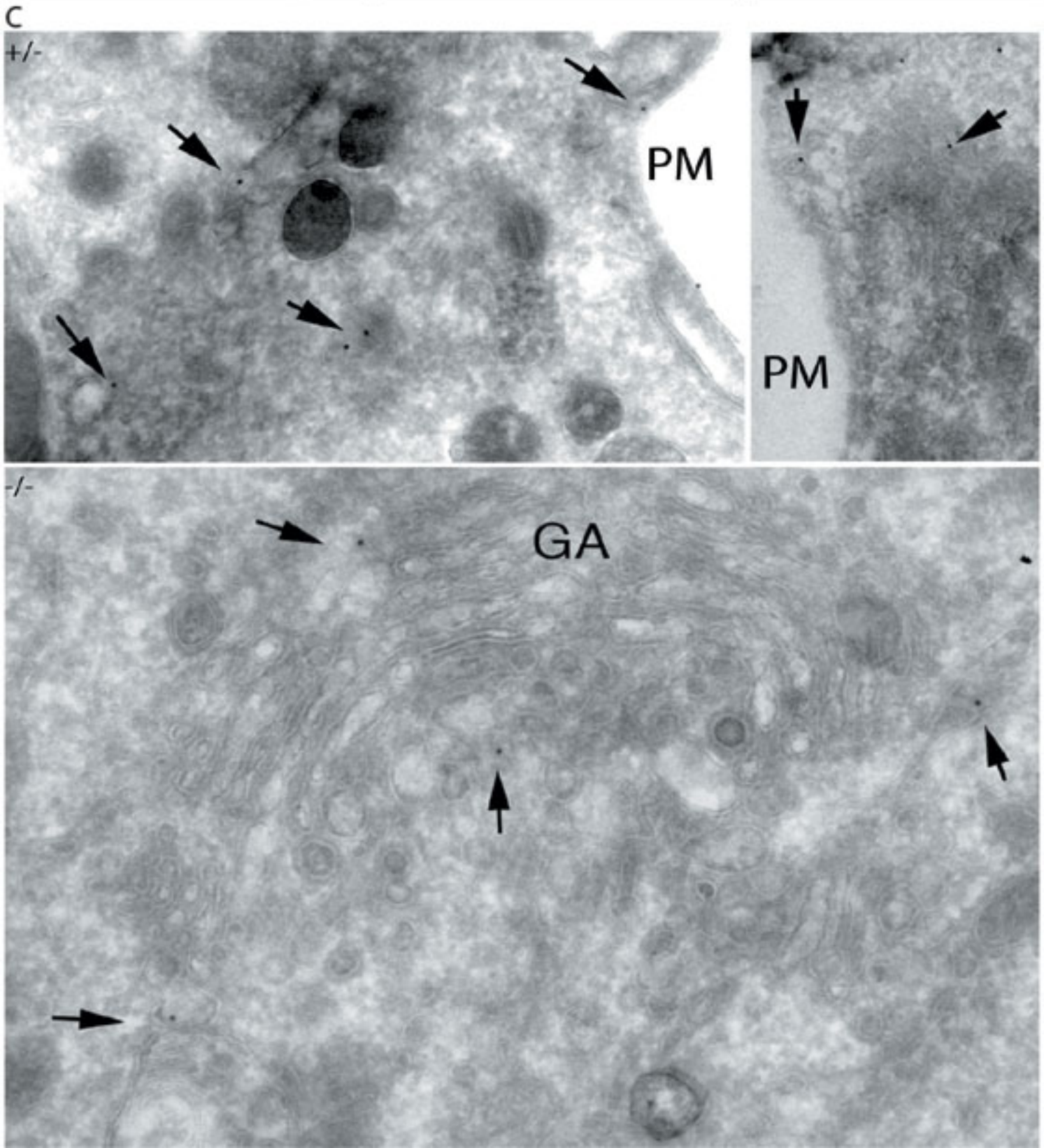
+/-
PM
PM
-/-
GA

Fig. 6. TI-VAMP concentrates in synapses in cultured granule cells and accumulates in the Golgi of mature *mocha* pyramidal neurons. (*a*) Granule cells (21 div) from control mice were colabeled with antibodies against TI-VAMP, Syp, and MAP2. TI-VAMP colocalizes with Syp (67.20+/-, 6.65% TI-VAMP-positive punctae are also Syp-positive, 10 cells, 1,282 synapses), suggesting it is present in a large subset of synaptic terminals. Postsynaptic neurons contacted by Syp+ terminals (neuron, n) were identified on the basis of the MAP2 staining to exclude astroglial (glial, g) staining of TI-VAMP. (*b*) Hippocampal neurons (14 div) cultured from control (+/-) or *mocha* (-/-) mice were colabeled with antibodies against TI-VAMP and antibodies against VAMP4. In *mocha* neurons, TI-VAMP accumulates in the Golgi, where it colocalizes with VAMP4. (Scale bar = 10 μm.) (*c*) Ultrathin cryosections of mature cultured hippocampal neurons (14 div) from control or *mocha* mice were immunogold labeled with polyclonal antibodies against TI-VAMP. In control (+/-) neurons, TI-VAMP is present on vesicles and tubules throughout the soma and occasionally present at the plasma membrane, whereas in *mocha* (-/-) neurons, TI-VAMP labeling is mainly found associated with the Golgi apparatus (GA).

a

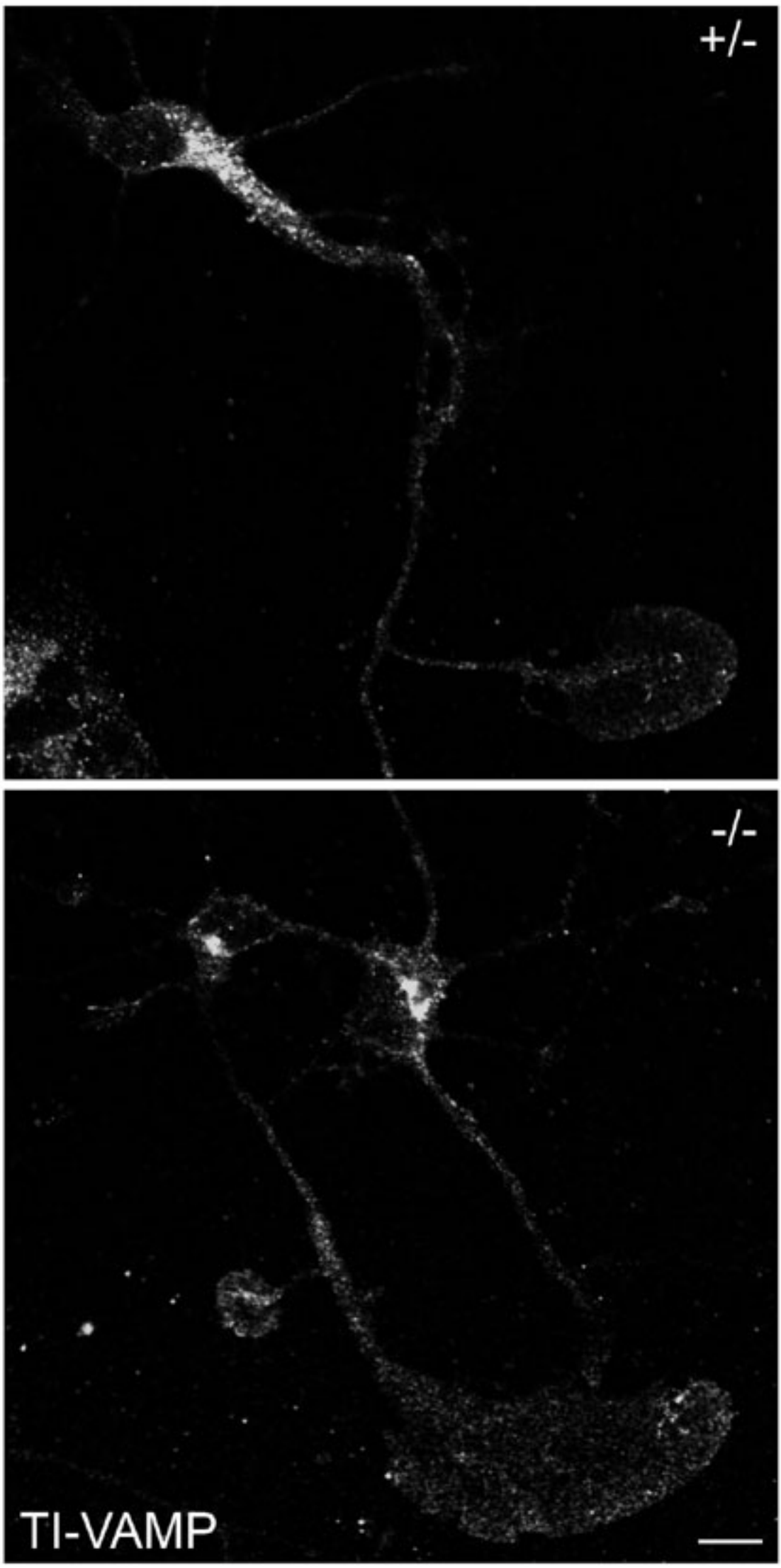

b

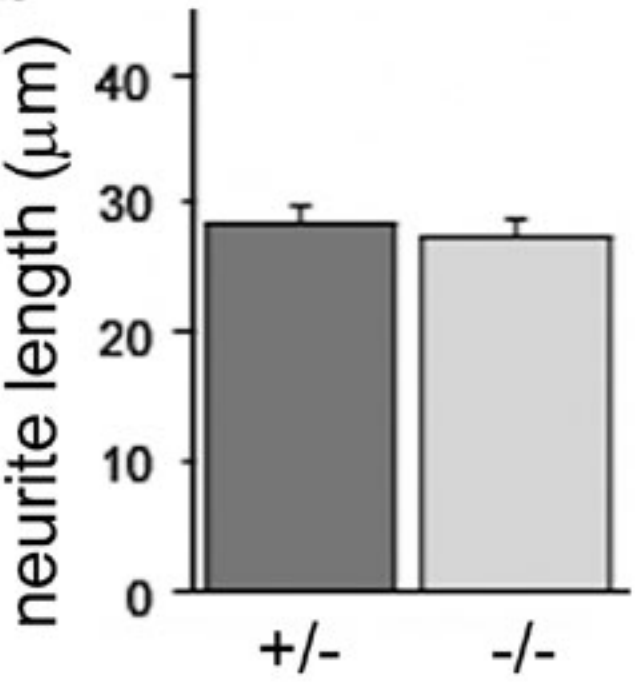

c

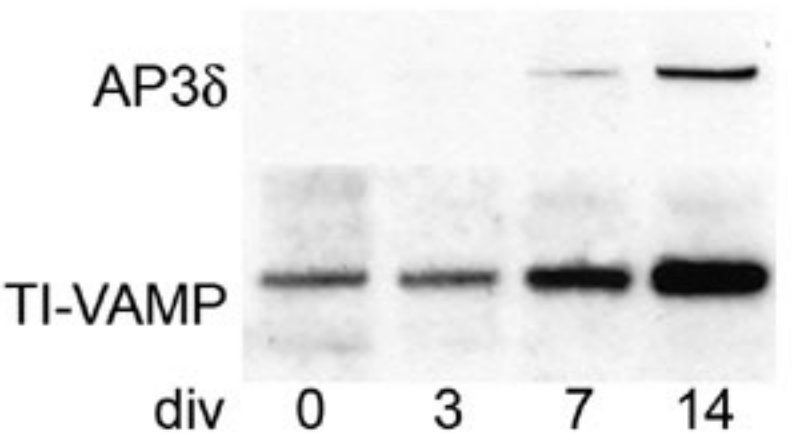

Fig. 7. Neurite outgrowth and TI-VAMP localization to the growth cone are unaffected in mocha neurons. (*a*) Immature hippocampal neurons (3 div) cultured from control (+/-) or *mocha* (-/-) newborn mice were labeled for TI-VAMP and analyzed by confocal microscopy. In both control and *mocha* neurons, TI-VAMP labeling is present in the growth cone. (Scale bar = 10 μm.) (*b*) Hippocampal neurons from control (+/-) and *mocha* (-/-) mice were grown for 1 div, and their neurite length was measured. No difference in neurite outgrowth was observed between control and *mocha* neurons (Bars represent SEM; $n = 100$ neurons from two independent experiments). (*c*) Hippocampal neurons growing in culture were lysed at different stages in development, and TI-VAMP and AP3 expression was analyzed by Western blotting. An equal quantity of protein was loaded in each lane. Note that both TI-VAMP and AP3 expression is up-regulated during development.

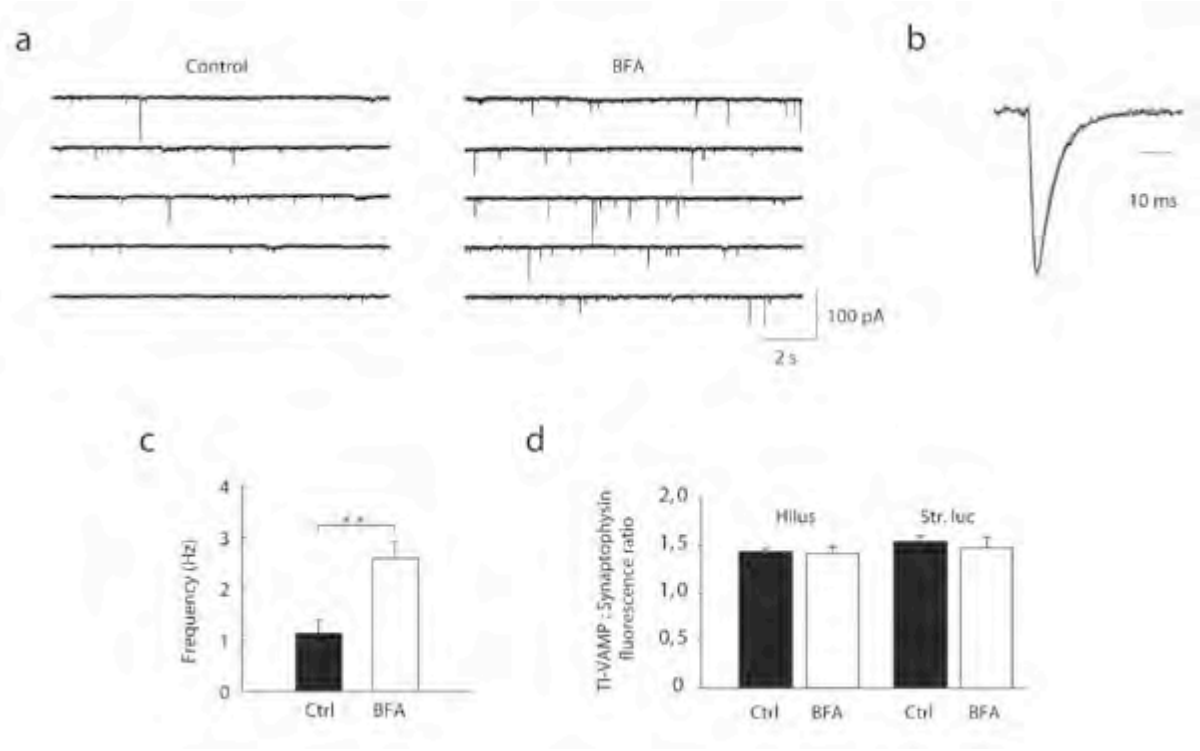

Fig. 8. Increased quantal release at mossy fiber (MF) terminals after acute disruption of AP3 by brefeldin A. (*a*) Sample traces from individual recordings of mEPSCs recorded from CA3 pyramidal cells in acute hippocampal slices (P10-12). Before recording, slices were incubated for >2 h in either normal ACSF or ACSF containing 10 μM brefeldin A. In brefeldin-treated slices, mEPSC frequency was increased by »127%, as compared to control (2.59 ± 0.33 vs. 1.14 ± 0.25 Hz; $n = 14$ and 12 cells, respectively; $P < 0.005$). (*b*) Scaled and averaged mEPSCs (»100) detected from the recordings shown in *a*. Black traces, control; blue traces. brefeldin A. No difference in either their rate of onset or decay was apparent. (*c*) Summary data from all recordings. (*d*) Ratio of TI-VAMP:Syp fluorescence intensity in control and BFA-treated slices in the hilus and stratum lucidum (mean ± SEM, $n = 14$ slices).

Supporting Text

Late onset of AP-3 expression explains normal mocha *brain development*

Our previous studies demonstrated that TI-VAMP is critical for neurite outgrowth (1, 2). Although brain development of the *mocha* mice seemed normal (3), such a defect may impair hippocampal connectivity and therefore complicate the interpretation of our present results. We thus examined TI-VAMP localization and neuritogenesis in control and *mocha* neurons (Fig. 7 *a* and *b*). Both neurite outgrowth and TI-VAMP localization to the growth cone were normal in hippocampal neurons cultured 1 to 3 days *in vitro* (div) from *mocha* mice (Fig. 7 *a* and *b*), demonstrating that TI-VAMP is transported to the growth cone in an AP3-independent manner. The lack of function of AP3 in neuritogenesis is further supported by the developmental regulation of its expression. In neurons growing in culture, AP3-δ expression was greatly increased at 7 days *in vitro* and reached a peak at »14 days (Fig. 7*c*). These results are thus consistent with both the essential role for TI-VAMP in neurite outgrowth and the fact that brain development appears normal in *mocha* mice, suggesting a role of AP3 in synaptic vesicles (SV) recycling rather than neurite outgrowth.

Material and Methods

Antibodies and reagents

The mouse monoclonal antibody (clone 158.2; ref. 4) and rabbit polyclonal antibody directed against TI-VAMP (TG18; ref. 5), the rabbit polyclonal antibodies antisynaptophysin (MC1; ref. 6), anti-VAMP4 (TG19; ref. 7), and anti-SNAP-25 (MC9; ref. 8) have been described. Mouse monoclonal antibodies against Syb2 (clone 69.1), Rab3a (clone 42.2), and Synaptotagmin 1 (clone 41.1) were generous gifts from R. Jahn (Max Planck Institute, Goettingen, Germany). Monoclonal antibody against tetanus neurotoxin (TeNT) has been described (9). Monoclonal anti-AP3δ antibody (SA4) was from the Developmental Studies Hybridoma Bank (University of Iowa, Iowa City, IA). Chicken polyclonal antibody against MAP2 (ab5392) was from AbCam (Milton Road, Cambridge, U.K.). Affinity-purified horseradish peroxidase-, Cy3-, Cy5-coupled, and biotin-coupled goat anti-rabbit, and anti-mouse immunoglobulins were from Jackson ImmunoResearch (West Grove, PA). Alexa 488- and 594-coupled goat anti-rabbit and anti-mouse immunoglobulins and Alexa 568-coupled phalloidin were from Molecular Probes (Carlsbad, CA). TeNT was isolated and characterized as described (10).

Neuronal cell culture and immunocytochemistry

Hippocampal neurons from newborn [postnatal day (P)0-P1] mice were prepared as described (11) and grown on poly-l-lysine-coated (Sigma-Aldrich, Saint Quentin Fallavier, France) 14-mm coverslips at a density of 25,000-50,000 per coverslip in Neurobasal media supplemented with B27 (GIBCO, Invitrogen, Cergy Pointoise, France) and Cytosine β-d-arabinofuranoside (Sigma-Aldrich).Granule cells were obtained by dissecting dentate gyrus on 1-mm-thick slices of postnatal (P5) hippocampus (12, 13). Granule cells were then processed as described (12) and grown on poly-Ornithine-coated (Sigma-Aldrich, France) per 14-mm coverslips at a density of 250,000 per coverslip in Neurobasal media supplemented with B27 (GIBCO, Invitrogen, France)/2 mM glutamine/25% horse serum for the first 5 div, 10% thereafter. Neurons in culture were fixed with 4% paraformaldehyde/4% sucrose and processed for immunofluorescence microscopy as described (5).

Electrophysiological recordings

For recording, cultures were transferred to a submerged chamber mounted on an upright microscope and superfused at a rate of »2.5 ml/min with artificial cerebrospinal fluid (ACSF) containing 124 mM NaCl, 26.2 mM $NaHCO_3$, 11 mM d-glucose, 2.5 mM KCl, 1 mM NaH_2PO_4, 4 mM $CaCl_2$, 4 mM $MgCl_2$. Whole-cell recordings from CA3 or CA1 pyramidal cells were made by using patch electrodes (3-5 MΩ resistance) made from borosilicate glass capillaries (Hilgenberg, Malsfeld, Germany) and filled with internal solution containing 110 mM $CsCH_3SO_3$, 20 mM CsCl, 10 mM Hepes, 10 mM EGTA, 4 mM MgATP, 0.4 mM Na_3GTP, and 1.8 mM $MgCl_2$.

Postsynaptic currents were evoked at 0.1 Hz by using extracellular stimulation through a borosilicate microelectrode filled with ACSF and recorded from cells held at -60 mV using an Axopatch 1D amplifier and digitized at 20 kHz using Clampex software of the pClamp 9 suite (Axon Instruments, Union City, CA). Postsynaptic current (PSC) amplitude and access resistance were monitored online. PSCs were then measured offline by using Clampex software. Currents were integrated over a 200-ms time window set immediately after the stimulus artifact (C_{200}). To correct evoked PSC charge for spontaneous PSCs, baseline currents were also integrated from a 50-ms prestimulus period, and the corrected charge was calculated as $C_{corr} = C_{200} - 4 \acute{} C_{50}$.

mEPSCs were recorded in modified ACSF in which $CaCl_2$ and $MgCl_2$ concentrations were adjusted to 0.5 and 4.5 mM, respectively, in the presence of tetrodotoxin (TTX, 2 μM, Latoxan, Valence, France) and bicuculline methochloride (20 μM, Fisher Bioblock Scientific, Illkirch, France). For focal application of a hypertonic solution, a second patch pipette filled with 0.5 M sucrose in ACSF was positioned in stratum lucidum »40-50 μm apart from the recorded cell and connected to a PicoSpritzer device (General Valve, Fairfield, NJ). mEPSCs were detected using Detectivent software written under LabView (kindly provided by N. Ankri, Institut National de la Santé et de la Recherche Médicale

U641, Marseille, France).

In some experiments, acute hippocampal slices were prepared from 12- to 14-day-old pups, as described (14). Slices were kept »1 h in normal ACSF equilibrated with a 95% O_2/5% CO_2 mixture. Half of the slices were then exposed to 10 μg/ml brefeldin A (Sigma) for an additional 2 h, whereas the other half was kept in ACSF until recordings were started.

Electron microscopy

Neurons from control or *mocha* mice were fixed with 2% (wt/vol) paraformaldehyde (PFA) or with a mixture of 2% (wt/vol) PFA and 0.2% (wt/vol) glutaraldehyde in 0.1 M phosphate buffer (PB), pH 7.4. Cells were processed for ultracryomicrotomy as described (15). Ultrathin sections were prepared with an Ultracut FCS ultracryomicrotome (Leica, Vienna, Austria), and single immunogold labeled with antibodies and protein A coupled to 10 or 15 nm of gold (PAG 10 and PAG 15). Sections were observed and photographed under a Philips CM120 Electron Microscope (FEI, Eindhoven, The Netherlands). Digital acquisitions were made with a numeric Keen View camera (Soft Imaging System, Münster, Germany).

Neurite outgrowth measurements

Neurons were fixed at 1 div, labeled with Alexa-568-coupled phalloidin, and imaged with a MicroMax CCD camera (Princeton Instruments, Princeton, NJ). Neurite length was measured using Metamorph software (Princeton Instruments).

1. Alberts P, Rudge R, Hinners I, Muzerelle A, MartinezArca S, Irinopoulou T, Marthiens V, Tooze S, Rathjen F, Gaspar P, *et al.* (2003) *Mol Biol Cell* 14:4207-4220.

2. Martinez-Arca S, Coco S, Mainguy G, Schenk U, Alberts P, Bouille P, Mezzina M, Prochiantz A, Matteoli M, Louvard D, Galli T (2001) *J Neurosci* 21:3830-3838.

3. Kantheti P, Qiao X, Diaz ME, Peden AA, Meyer GE, Carskadon SL, Kapfhamer D, Sufalko D, Robinson MS, Noebels JL, *et al.* (1998) *Neuron* 21:111-122.

4. Muzerelle A, Alberts P, Martinez-Arca S, Jeannequin O, Lafaye P, Mazie J-C, Galli T, Gaspar P (2003) *Neuroscience* 122:59-75.

5. Coco S, Raposo G, Martinez S, Fontaine JJ, Takamori S, Zahraoui A, Jahn R, Matteoli M, Louvard D, Galli T (1999) *J Neurosci* 19:9803-9812.

6. Chilcote TJ, Galli T, Mundigl O, Edelmann L, McPherson PS, Takei K, De Camilli P (1995) *J Cell Biol* 129:219-231.

7. Mallard F, Tang BL, Galli T, Tenza D, Saint-Pol A, Yue X, Antony C, Hong W, Goud B, Johannes L (2002) *J Cell Biol* 156:653-654.

8. Garcia EP, McPherson PS, Chilcote TJ, Takei K, De Camilli P (1995) *J Cell Biol* 129:105-120.

9. Sweeney ST, Broadie K, Keane J, Niemann H, O'Kane CJ (1995) *Neuron* 14:341-351.

10. Weller U, Mauler F, Habermann E (1988) *Naunyn Schmiedebergs Arch Pharmacol* 338:99-106.

11. Chang S, De Camilli P (2001) *Nat Neurosci* 4:787-793.

12. Boss BD, Gozes I, Cowan WM (1987) *Brain Res* 433:199-218.

13. Gomez-Lira G, Lamas M, Romo-Parra H, Gutierrez R (2005) *J Neurosci* 25:6939-6946.

14. Scheuber A, Miles R, Poncer JC (2004) *J Neurosci* 24:10402-10409.

15. Raposo G, Kleijmer KJ, Posthuma G, Slot JW, Geuze HJ (1997) in *Handbook of Experimental Immunology*, eds Herzenberg LA, Weir DM, Blackwell C (Blackwell, Malden, MA), pp 1-11.